OPTIMIZED 2D ARRAY DESIGN FOR ULTRASOUND IMAGING

Bakary Diarra[1,2], Hervé Liebgott[1] , Marc Robini[1], Piero Tortoli[2] , Christian Cachard[1]

[1]CREATIS, Université de Lyon ; CNRS UMR 5220 ; INSERM U1044 ; Université Lyon 1 ; INSA-Lyon, Villeurbanne, France,

[2]Electronics and Telecommunications Dept., Università degli Studi di Firenze, Italy

ABSTRACT

Ultrasound imaging is one of the least expensive and safest diagnostic modalities routinely used. An attractive recent development in this field is three-dimensional (3D) imaging with two-dimensional (2D) matrix probes. The difficulty in implementing these probes comes from their large number of elements; for instance, the probe considered in this paper is composed of 1024 elements, whereas the number of channels of most current beamformers ranges from 64 to 256. To reduce the number of active elements, we propose a new sparse array design technique based on simulated annealing. Our method is capable of significantly reducing the number of probe elements as well as the side lobe level in a reasonable amount of computing time. Experiments in the context of hepatic biopsy show that good imaging performance can be obtained with only 177 active elements out of the total of 1024.

Index Terms— *ultrasound*, 2D array, sparse array, simulated annealing

1. INTRODUCTION

In 3D ultrasound imaging, experiments are mostly conducted with 3D mechanical probes. In a recent publication, Uherčík et al. [1] propose an algorithm for needle detection based on a 3D mechanical scanning probe. The detection algorithm based on a RANSAC procedure is fast and accurate, but the volume acquisition time is a severe limitation for this application. An interesting alternative is electronically controlled 2D matrix arrays. However, the control of such arrays is a technical challenge because of the too large number of elements to be connected. Among the various methods proposed to reduce the number of active elements, the most promising is the sparse array technique [2]. This approach, however, deteriorates the beam pattern compared to the original dense array. Another problem involves the side lobes and the grating lobes (linked to the element periodicity in the array and to the element size), which are undesired parts of the emitted beam. These lobes cause image artifacts and must be as low as possible to obtain good image resolution. The new sparse array design technique proposed herein intends to limit the amplitude of the side lobes while minimizing the number of necessary active elements. The core of our method is based simulated annealing.

This paper is organized as follows. Section 2 describes the choice of the probe parameters and various element reduction techniques, Section 3 presents the optimization algorithm together with experimental results, and our conclusions are given in Sections 4.

2. PROBE DESIGN AND REDUCTION TECHNIQUES

Theoretically, to limit the amplitude of the grating lobes, the pitch d (that is, the inter-element distance) must be smaller than half the wavelength in the elevation and lateral directions, that is,

$$d \leq \lambda / 2 , \qquad (1)$$

where λ denotes the wavelength.

The main parameters of the probe (see Fig. 1) are chosen based on the characteristics of the tissue region to be explored. We consider the case of the liver inspection: the frequency commonly used in liver imaging is 3.5 MHz [3], which corresponds to a wavelength λ of 0.44 mm. Condition (1) is satisfied at the expense of a widening of the main lobe, and a pitch value slightly above half the wavelength is a good tradeoff: we chose $d = 0.6\,\lambda$. The elements are squares of size $w_d = 0.5\,\lambda$ and the space between two consecutive elements (the kerf) is $0.1\,\lambda$. The probe elevation dimension must be smaller than the intercostal distance, which is about 5 mm, to avoid reflection on ribs and the formation of image artifacts. For the chosen pitch value, the number of elements in the elevation direction is 22. For electronic adaptability, this number is reduced to 16. The number of elements in the lateral direction is 64, so that the resulting probe contains $N = 64\times16 = 1024$ elements. However, since the typical channel number of beamformers does not exceed 256, the number of elements to connect must be decreased without excessive deterioration of the output image features.

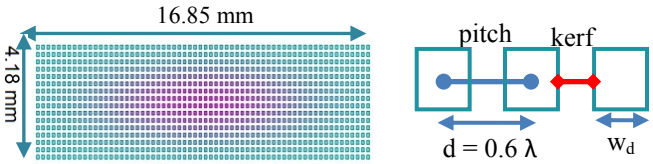

Fig. 1. Probe dimensions (element apodization decreases from the center to the edges).

Various techniques have been proposed to reduce the number of elements to connect; the most widely used are edge-element deactivation and sparse array techniques, which are discussed below.

2.1 Edge-element deactivation

The technique proposed by Turnbull *et al* [4] consists in deactivating edge elements so that only the circular (or ellipsoidal for a non-squared array) part of the matrix remains (see Fig. 2(a)). Moving from a rectangular to an ellipsoidal aperture reduces the number of elements by approximately 30% [5].

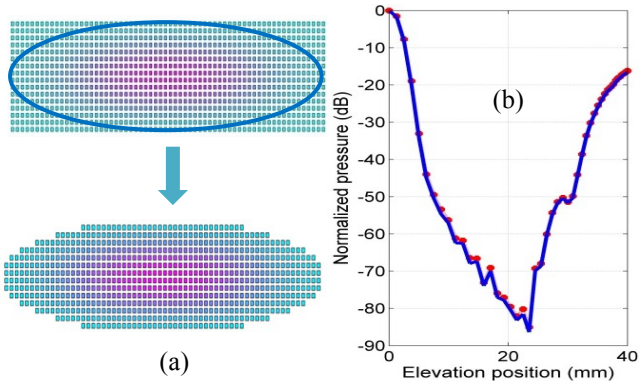

Fig. 2. Ellipsoidal part of a 64×16 array and associated beam profiles before (continuous line) and after (dotted line) edge-element deactivation.

Using this technique, the initial array of 1024 elements is reduced to $N' = 728$ elements (that is, a 29% reduction). The associated beam profile is shown in Fig. 2(b). (Note that all the beam profiles presented in this paper are simulated using Field II [6][7] and are displayed by plotting the maximum pressure along the A-lines of the volume scanned in the lateral and elevation direction.) This profile is well preserved because the contribution of the deactivated peripheral edge elements is low. However, the reduction of the number of elements resulting from this deactivation technique is not sufficient; it must be combined with a sparse array technique to be below the upper limit of 256 active elements.

2.2 Sparse array techniques

Sparse array techniques periodically or randomly deactivate some elements of the 2D array. The periodical version presents a good beam pattern in terms of main lobe width and pressure intensity, but the unwanted side lobes are prominent [8]. The random sparse array technique (illustrated in Fig. 3) is more promising because it produces a lower side lobe level while maintaining an acceptable main lobe width. Using this approach, the local inter-element distance can reach several times the pitch of the dense array, which has consequences on the side lobe appearance and on the width of the main lobe. To limit the effect of the reduction of the number of element on the beam pattern, the sparse array technique can be combined with an optimization algorithm to constrain the side lobe amplitude and to prevent widening of the main lobe [5] [9].

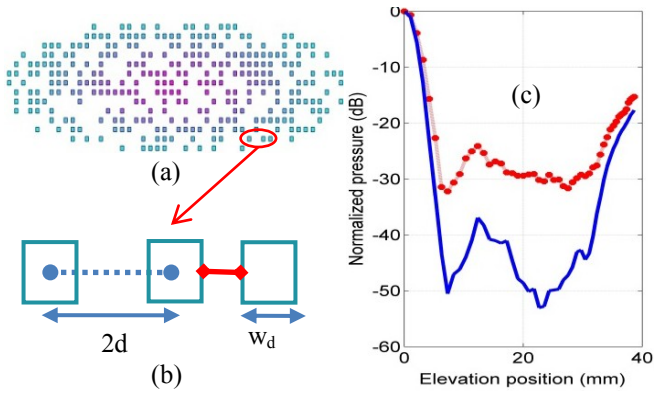

Fig. 3. (a) Random sparse array, (b) local inter-element distance increase, and (c) beam profiles for 260 elements (continuous line) and 140 elements (dotted line) illustrating the effect on the appearance of the side lobe and on the width of the main lobe.

Fig. 3(c) shows that the lower the number of elements, the higher the side lobe level and the wider the main lobe, which can hinder image quality. To reduce the number of elements without deteriorating the beam profile, we use a new approach based on simulated annealing that we compare to the approach presented in [9].

3. Optimization by Simulated Annealing

There are several algorithms for optimizing element deactivation; many of them are detailed in [10] together with their simulation results. All these methods aim to reduce the side lobe level while maintaining the width of the main lobe constant. The most frequently used methods are simulated annealing and genetic algorithms. For large 2D arrays, simulated annealing is preferred for its robustness and its lower computational cost [11].

3.1 The simulated annealing algorithm

Simulated annealing (SA) is a generic method for combinatorial optimization that is quite popular because of its ease of implementation and its global convergence properties. The key feature of SA is that it allows uphill moves (that is, moves that increase the value of the objective function) in order to escape local minima. By analogy with the physical process of annealing in solids, uphill moves are accepted with a certain probability controlled by a temperature parameter that decreases monotonically to zero.

Without going into detail, an SA algorithm with cost function f is a Markov chain $(X_n)_{n\geq 0}$ whose transitions are guided by a communication mechanism θ and controlled by a cooling sequence $(T_n)_{n>0}$. The communication mechanism gives the probabilities of the possible moves for generating a candidate solution from the current solution, and the cooling sequence is a divergent sequence of temperatures. The transitions of $(X_n)_{n\geq 0}$ are defined as follows: for any (x, y) such that $x \neq y$,

$$P(X_n = y \mid X_{n-1} = x) = \begin{cases} \theta(x,y) & \text{if } f(y) \leq f(x) \\ \theta(x,y)\exp(-(f(y)-f(x))/T_n) & \text{if } f(y) > f(x) \end{cases} . \quad (2)$$

Simply put, downhill moves are unconditionally accepted, whereas an uphill move from x to y is accepted with probability $\exp(-(f(y)-f(x))/T_n)$ at iteration n. As the temperature goes to zero, the distribution of X_n concentrates on the global minima of f, and the process converges to a global minimum if the temperature is inversely proportional to the logarithm of the iteration index [12]. However, logarithmic cooling yields extremely slow convergence and most successful applications of SA use exponential cooling, which is theoretically justified in [13]. In this study, we use an exponential cooling schedule of the form

$$T_n = 0.9^{\lfloor n/N' \rfloor} T_0, \tag{3}$$

where T_0 denotes the initial temperature value, $N' = 728$ is the number of remaining elements after deactivation of the peripheral elements of the initial 2D array, and $\lfloor \cdot \rfloor$ is the ceiling function.

3.2 Proposed objective function

The main parameters of our optimization problem are the number of activated elements and the maximum side lobe level; they must be included in the cost function. A general cost function was proposed in [9]. This function uses the pressure formulation established for the far field beam pattern of the I×J element probe by Nielsen et *al* [14]:

$$p(u,v) = \left| \sum_{i=1}^{I} \sum_{j=1}^{J} w_{i,j} \, e^{-j\frac{2\pi}{\lambda}(x_i u + y_j v)} \right|, \tag{4}$$

where $w_{i,j}$ is the activation coefficient of the element at position (i,j), x_i and y_j are the coordinates of the element at position (i,j), and u and v are the beam direction vectors.

We propose a new cost function that improves the cost function presented in [9] and that allows setting the maximum side lobe level. This cost function uses the l_1-norm of the element coefficients and produces sparser arrays than those obtained via the formulation in [9] and [11]. It is defined by

$$f(W) = \left[\sum_{(u,v)\in S} \left(\frac{p(u,v)}{A} - p_d(u,v) \right) \right]^2 + \alpha \sum_{i,j} |w_{i,j}|, \tag{5}$$

where W is the matrix of the coefficients $w_{i,j} \in [0, 1.5]$ of the 2D array, A is the maximum pressure, p_d is the maximum side lobe level, S denotes the area excluding the main lobe and satisfying $p(u,v)/A > p_d(u,v)$, and $\alpha \in]0\ 1[$ adjusts the strength of the stabilization term $\sum_{i,j}|w_{i,j}|$.

Compared to the stabilization term proposed in [9] and [11] (which uses binary variables), ours has the advantage of being continuous and convex, which translates to an optimization problem of lower complexity. Note that since the activation coefficients $w_{i,j}$ in (5) are multi-valued, we define a threshold τ such that an element (i,j) is active if $w_{i,j} \geq \tau$ (we set $\tau = 0.2$ in our experiments). The number of elements must be lower than 256, which is generally manageable and also suitable to our experimental scanner, the ULA-OP [15].

3.3 Results and comparison

The initial temperature value is chosen large enough to accept most transitions at the beginning of the optimization process ($T_0 = 1000$), and the maximum number of sweeps is set to 500, where a sweep is a sequence of $N' = 728$ iterations. The constraints are the following: maximum side lobe level below − 40 dB and maximum width of the main lobe smaller than 0.3 mm (which is the mean value of the biopsy needle radius). The hyper-parameter α is set empirically: we consider the value that produces the best result, that is, $\alpha = 4\times10^{-5}$ in the present case.

The results produced by Trucco's algorithm and ours are summarized in Table 1 and displayed in Figs. 4(a) and 4(b). Both algorithms were stopped when the number of active elements is kept unchanged during several sweeps. Using our approach, the 1024-elements initial array is reduced to a 177-elements array (that is, an 82% reduction) that satisfies the constraints. The width of the main lobe at − 6 dB is 0.2 mm and the side lobes remain lower than − 40 dB. This is acceptable for biopsy operations, as the radius of the needle varies from 0.18 mm to 0.3 mm. The solution produced by Trucco's method also satisfies the constraints, but it has 58 more active elements and its computation took 90 additional sweeps. Fig. 4(c) displays the evolution of the number of active elements as a function of the number of sweeps for the two methods. The beam profiles of the optimized probes obtained with the two methods are shown in Fig. 5.

The capabilities of the sparse array produced by the proposed method is assessed in a practical situation by imaging a biopsy needle with 0.3 mm radius and 16 mm length inserted obliquely into a phantom. The result is displayed in Fig. 6, where the needle appears as a thin high scatter density region in the phantom. The visualization of the needle in both the lateral and elevation directions is clearly acceptable.

Method	Side lobes	Active elements	Main lobe (− 6 dB)	Sweeps
Trucco's	− 40 dB	235	0.2 mm	271
ours	− 40 dB	177	0.2 mm	181

Table 1: Comparisons of the results obtained with Trucco's method and with the proposed method.

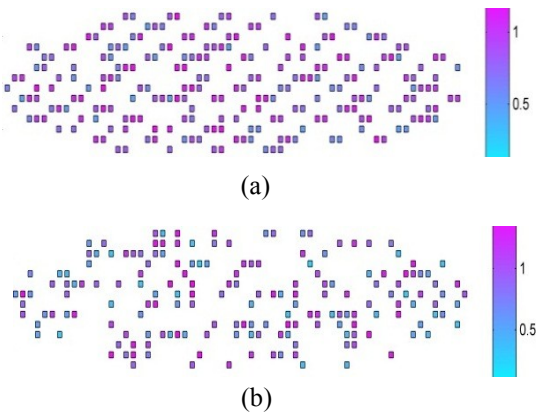

(a)

(b)

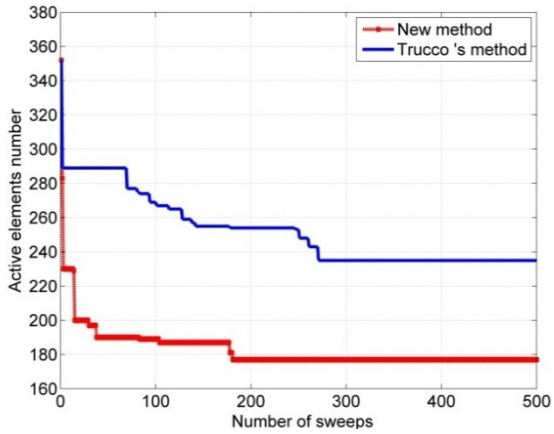

(c)

Fig. 4. (a) Sparse array produced by Trucco's method [9]; (b) sparse array obtained with our method; (c) number of active elements as a function of the number of sweeps.

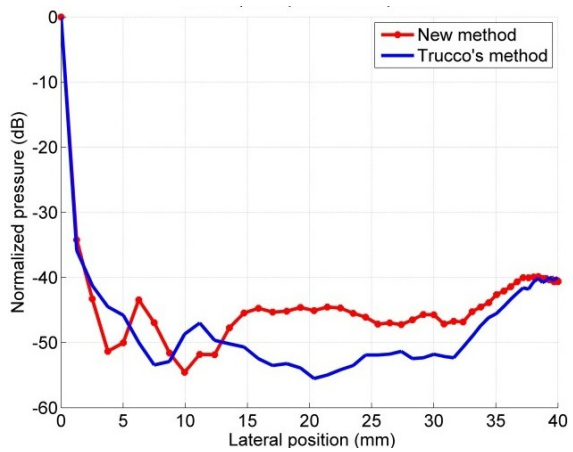

Fig. 5. Beam profiles of the sparse arrays obtained with the proposed method (dotted line) and with Trucco's method (continuous line).

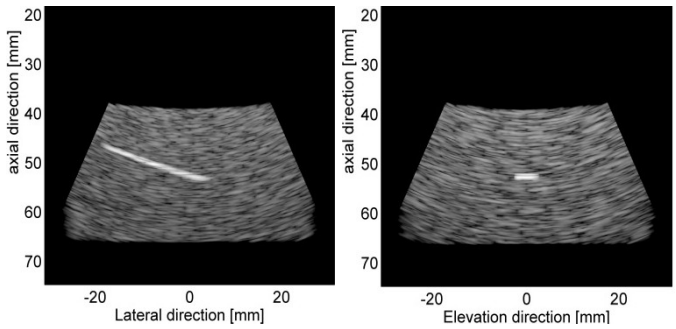

(a) (b)

Fig. 6. Needle detection with the 177-elements probe obtained with our method: (a) lateral direction; (b) elevation direction.

3.4 Discussion

The number of active elements of a 2D array probe has a great impact on its beam characteristics. Because of technical constraints, this number must be small compared to the total number of elements, but this deteriorates the beam pattern by creating side lobes and widening the main lobe. Simulated annealing alleviates these drawbacks by minimizing the specific cost function given in (5), which includes the constraints to be satisfied. The effect of the constant α that multiplies the stabilization term is important: it should be large enough to reduce the number of active elements significantly, but not too large, as the constraints embedded in the first term of the cost function are not satisfied otherwise. The proposed approach can be used to optimize large 2D arrays in a reasonable amount of computing time.

4. Conclusion

This paper deals with the specification of a probe dedicated to biopsy applications. To design a probe with a small number of active elements, the sparse array technique is a promising approach that requires solving a difficult optimization problem. The new sparse array optimization method presented here is compared to that proposed by in [9]; our results show greater reduction of the number of active elements and faster convergence. Using our approach, the initial 1024-elements 2D array is reduced to 177 elements (82% reduction) in 181 sweeps, where as it is reduced to 235 elements (77% reduction) in 271 sweeps using the method in [9]. The optimized 2D array was tested by simulating the detection of a needle inserted in a phantom and the results show the target clearly. An experimental probe will be designed in the future to assess the improvement brought by the new method in practical situations.

Acknowledgments

This work was partially supported by the Centre Lyonnais d'Acoustique (CeLyA), under ANR grant no. 2011-LABX-014

The first author is financially supported by the Franco-Italian University (VINCI and Galilee grants) and by the Rhone-Alpes region (Explora'Doc grant).

5. REFERENCES

[1] M. Uherčík, J. Kybic, H. Liebgott, et C. Cachard, « Model Fitting Using RANSAC for Surgical Tool Localization in 3-D Ultrasound Images », *Biomedical Engineering, IEEE Transactions on*, vol. 57, n°. 8, p. 1907-1916, 2010.

[2] M. Ezhilarasi, M. Rajaram, et S. . Sivanandham, « Fractal Geometry in 2D Matrix Array for Realtime 3D Ultrasound Imaging », *Calicut Medical Journal 2008*, vol. 6, 2008.

[3] N. N. Lee, R. W. O'Rourke, J. Cheng, et P. D. Hansen, « Transthoracic hepatic radiofrequency ablation », *Surg Endosc*, vol. 18, n°. 11, p. 1672-1674, oct. 2004.

[4] D. H. Turnbull et F. S. Foster, « Beam steering with pulsed two-dimensional transducer arrays », *Ultrasonics, Ferroelectrics and Frequency Control, IEEE Transactions on*, vol. 38, n°. 4, p. 320-333, 1991.

[5] B. Diarra, H. Liebgott, P. Tortoli, et C. Cachard, « 2D matrix array optimization by simulated annealing for 3D hepatic imaging », *IEEE International Ultrasonics Symposium*, Orlando, Florida,USA, p. in press, oct-2011.

[6] J. A. Jensen, « FIELD: A Program for Simulating Ultrasound Systems », *10TH NORDICBALTIC CONFERENCE ON BIOMEDICAL IMAGING VOL 4 SUPPLEMENT 1 PART 1 351–353*, vol. 34, n°. Supplement 1, Part 1, p. 351-353, 1996.

[7] J. A. Jensen et N. B. Svendsen, « Calculation of pressure fields from arbitrarily shaped, apodized, and excited ultrasound transducers », *IEEE Transactions on Ultrasonics, Ferroelectrics and Frequency Control*, vol. 39, n°. 2, p. 262-267, mars 1992.

[8] A. Austeng et S. Holm, « Sparse 2-D arrays for 3-D phased array imaging - design methods », *Ultrasonics, Ferroelectrics and Frequency Control, IEEE Transactions on*, vol. 49, n°. 8, p. 1073-1086, 2002.

[9] A. Trucco, « Thinning and weighting of large planar arrays by simulated annealing », *IEEE Trans. Ultrason., Ferroelect., Freq. Contr.*, vol. 46, n°. 2, p. 347-355, mars 1999.

[10] S. Holm, A. Austeng, et K. Iranpour, « Sparse sampling in array processing », 2009.

[11] P. Chen, B. Shen, L. Zhou, et Y. Chen, « Optimized simulated annealing algorithm for thinning and weighting large planar arrays », *J. Zhejiang Univ. - Sci. C*, vol. 11, n°. 4, p. 261-269, avr. 2010.

[12] B. HAJEK, « Cooling schedules for optimal annealing », *Mathematics of operations research*, vol. 13, n°. 2, p. 311-329.

[13] O. Catoni, « Rough Large Deviation Estimates for Simulated Annealing: Application to Exponential Schedules », *Ann. Probab.*, vol. 20, n°. 3, p. 1109-1146, juill. 1992.

[14] R. O. Nielsen, *Sonar Signal Processing*. Artech House Publishers, 1991.

[15] P. Tortoli, L. Bassi, E. Boni, A. Dallai, F. Guidi, et S. Ricci, « ULA-OP: an advanced open platform for ultrasound research », *IEEE Transactions on Ultrasonics, Ferroelectrics and Frequency Control*, vol. 56, n°. 10, p. 2207-2216, oct. 2009.